JOURNAL OF MATERIALS SCIENCE 21 (1986) 803–809

Orientation in poly(ethylene terephthalate) drawn by solid state coextrusion

TONG SUN*, C. RICHARD DESPER‡, ROGER S. PORTER
Polymer Science and Engineering Department, Materials Research Laboratory, University of Massachusetts, Amherst, Massachusetts 01003, USA

The development of uniaxial orientation by solid-state extrusion at 60 to 90° C has been evaluated for both the amorphous and crystalline components of a poly(ethylene terephthalate). Analyses involved X-ray diffraction, birefringence and visable dichroism. The dichroism was evalulated from a host dye molecule. The initial PET film for draw was amorphous and isotropic. Orientation functions for the amorphous and the developed crystalline phases are reported at a series of draw ratios up to 4.4.

1. Introduction

Interest remains intense in the development of polymers of high modulus and strength. Poly(ethylene terephthalate) (PET) prepared by solid state extrusion is certainly a candidate [1]. The approach here has been extrusion of an amorphous film, below its glass-transition temperature, followed by annealing under tension [2].

Extensive work has been reported on molecular orientation and morphology deformation by conventional drawing processes of PET, both below and above T_g [3–10]. Conventional drawing of PET below T_g results in necking, so that the only samples readily attainable [3, 8] have been those for the natural draw ratio. In this study, we elucidate the development of orientation achieved by solid-state coextrusion for both crystalline and amorphous components (by using X-ray diffraction, birefringence and visible dichroism measurements). A series of ribbons uniformly drawn from isotropic, amorphous PET have been evaulated as a function of extrusion draw ratio, λ, and extrusion temperature, ET, both below and above T_g.

2. Experimental procedure

2.1. Sample

A PET film of $\sim 25\,\mu$m thickness was used for drawing. It was essentially amorphous ($\leqslant 2\%$ crystalline) and isotropic by density and birefringence. The PET $\bar{M}_n$ was ~ 14.500.

2.2. Coextrusion

The PET film was deformed by the split billet coextrusion technique in an Instron capillary rheometer as reported previously [11].

2.3. Crystallinity

Crystallinity was measured with a density gradient column using a carbon tetrachloride–heptane mixture at 25° C. The volume fraction crystallinity, X_v, was calculated assuming a crystal density, d_c of 1.455 and an amorphous density, d_a of 1.335 gm cm^{-3} as follows:

$$d = d_c X_v + d_a(l - X_v) \quad (1)$$

where d represents the density of the sample

2.4. Birefringence and average orientation function

The total birefringence, Δn, of PET films was measured with a Zeiss polarizing microscope equipped with a rotatable compensator and a quartz combination plate. The average orientation function of amorphous and crystalline regions, f_{av}, is given by

$$f_{av} = \frac{2\Delta n}{\Delta n_c^0 + \Delta n_a^0} \quad (2)$$

where Δn_c^0 and Δn_a^0 are the intrinsic birefringences of PET crystals and the ideal amorphous phase respectively, taken to be 0.22 and 0.275 [12].

2.5. Visible dichroism and amorphous orientation function

To evaluate the orientation of the amorphous PET, visible dichroisms of a PET–Disperse Yellow 7 system were measured [13, 14]. The undrawn amorphous film was dyed carefully from an aqueous solution of Disperse Yellow 7 at 50° C for 72 h. After dying, the films were washed thoroughly with 50° C distilled water, then rinsed with cold distilled water for 72 h and dried in a vacuum desiccator. As examined by density, X-ray, birefringence and dichroism measurements the dyed film was isotropic and amorphous. After coextrusion, polarized light absorbances parallel and perpendicular to the stretch direction, $A_\parallel$ and $A_\perp$, were measured at room temperature on a double beam Beckman spectrophotometer ACTA MVI at a scan speed of 1 nm sec^{-1}. A film treated exactly the same way as in the drawn sample but undyed was used as reference. Both absorbances ($A_\parallel$ and $A_\perp$) were measured at $\lambda = 405$ nm with the amorphous orientation function, $f_{a,d}$, calculated as follows:

*On leave from East China Institute of Textile Science and Technology, Shanghai, People's Republic of China.
‡US Army Materials and Mechanics Research Center, Polymer Research Group, Building 39, Watertown, Massachusetts 02172, USA.

0022–2461/86 $03.00 + .12

$$f_{a,d} = 1 - \tfrac{3}{2}\langle \sin^2\theta_1 \rangle$$
$$= \frac{A_\parallel - A_\perp}{A_\parallel + 2A_\perp} \frac{1}{[1 - \tfrac{3}{2}\sin^2\theta_2][1 - \tfrac{3}{2}\sin^2\theta_3]}$$
$$= \frac{A_\parallel - A_\perp}{A_\parallel + 2A_\perp} \frac{1}{D_2 \times D_3} \quad (3)$$

where θ_1 is the average inclination angle of amorphous segments to the stretch direction, Z.

θ_2 is the average angle between the axis of amorphous segments and the dye molecule.

θ_3 is the average angle between the dye molecule and its transition moment. The value of the product, $D_2 \times D_3$ in Equation 3 depends on the specified polymer-dye stuff system used. According to Okajima *et al.* [14], for the PET–Disperse Yellow 7 system the value of $D_2 \times D_3$ is unity and remains unchanged after stretching and heating.

2.6. Crystallite orientation function

Having found Δn and $f_{a,d}$, the crystallite function, f_c, can be obtained from the following expression:

$$f_c = \frac{\Delta n - \Delta n_a^0 f_{a,d}(1 - X_v)}{\Delta n_c^0 X_v} \quad (4)$$

2.7. X-ray diffraction and crystallite orientation functions

X-ray diffraction patterns were obtained using a Technology for Energy Corp. model 210 one-dimensional position-sensitive proportional counter (PSPC) connected to a Lecroy 3500M multiple channel analyser. The PSPC was mounted on the detector arm of a Picker model 3645 X-ray diffractometer, using an incident beam collimator of 0.5 mm diameter, at a distance of 290 mm from the specimen. To minimize air scattering, a knife edge beam stop was placed 3 mm from the specimen position. Angular calibration was achieved by measuring the suitably attenuated X-ray beam with the detector arm placed at a series of known angles near the $2\theta = 0°$ position. Radial patterns (intensity against Bragg angle 2θ) were determined using the detector mounted in the horizontal position, parallel to the motion of the detector arm, whereas partial azimuthal patterns were determined using the detector in the vertical position. The active detector dimensions are 1 cm wide × 10 cm high; at the 290 mm distance, the angular resolution was 0.3° in the longer dimension, with a divergence of ± 1° in the shorter dimension. The latter corresponds to the so-called vertical divergence of a conventional X-ray diffractometer. Data were corrected for local variation in detector efficiency.

Partial azimuthal patterns were obtained as the dependence of intensity on an elevation angle ε above the plane of scattering at a fixed Bragg angle 2θ. In earlier studies [15], the crystallite orientation distribution was determined as a function of the sample orientation angle χ. The two angles are not equivalent, but are related by

$$\tan(\chi - \chi_0) = \tan\varepsilon/(2\sin\theta) \quad (5)$$

where χ_0 is value of the latitude angle χ at the $\varepsilon = 0$ position and corresponds to the instrument angle of the same name for a three- or four-circle X-ray goniometer [16].

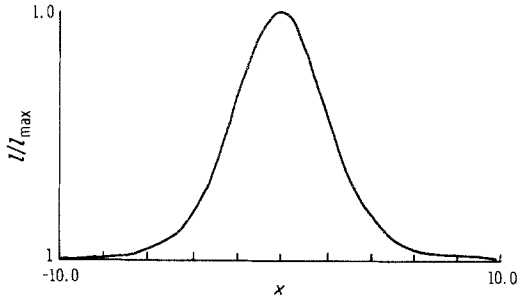

Figure 1 Orientation distribution of (1 1 0) plane of reference extruded polyethylene strand as determined by PSPC in vertical position.

Instrument performance was checked by obtaining data for the (1 1 0) orientation of an extruded polyethylene which had been previously studied using a receiving slit with a step-scanning program. Results were compared in terms of the value of the parameter $\chi_{1/2}$, the angular range between maximum and half-maximum intensity in the orientation distribution, as well in terms of the orientation function f_{110}. The orientation distribution determined by the new PSPC method is shown in Fig. 1, while the parameters are compared in Table I. The latter agree to within the expected precision [17] of 0.05° for $\chi_{1/2}$ and 0.0005 for f_{110}.

For evaluating the orientation functions of three principal crystallite axes ($f_{x,a}$, $f_{x,b}$ and $f_{x,c}$) the X-ray diffraction method can usually be used. In the present work, a cartesian coordinate system is superimposed on the crystal with the following definitions: **c** is parallel to the polymer chain direction, **a** is normal to the 1 0 0 plane, and **b** is perpendicular to both **a** and **c**. While differing from the usual triclinic coordinates for poly(ethylene terephthalate), this cartesian coordinate system is suitable for orientation analysis by the method of Wilchinsky. According to the Wilchinsky Equation [18] and the orthogonality condition as shown in Equations 6 and 7,

$$\langle \cos^2\phi_{hk0} \rangle = e_{hk0}^2 \langle \cos^2\delta \rangle + f_{hk0}^2 \langle \cos^2\varepsilon \rangle + 2e_{hk0}f_{hk0}\langle \cos\delta\cos\varepsilon \rangle \quad (6)$$

$$\langle \cos^2\delta \rangle + \langle \cos^2\varepsilon \rangle + \langle \cos^2\sigma \rangle = 1 \quad (7)$$

$f_{x,a}$, $f_{x,b}$ and $f_{x,c}$ can be evaluated by using three unique ($h\,k\,0$) crystallographic planes as follows. In this study the planes chosen are (1 0 0), (T 1 0) and (0 1 0).

$$f_{x,a} = \tfrac{1}{2}[3\langle \cos^2\delta \rangle - 1] \quad (8)$$

where

$$\langle \cos^2\delta \rangle = 1.00\langle \cos^2\phi_{100} \rangle \quad (9)$$

$$f_{x,b} = \tfrac{1}{2}[3\langle \cos^2\varepsilon \rangle - 1] \quad (10)$$

TABLE I Comparison of PSPC determination of orientation parameters with step-scanning method (extruded polyethylene reference sample)

Parameter	PSPC value	Step-scan value
$\chi_{1/2}$ (1 1 0)	2.45°	2.43°
f_{110}	-0.496_8	-0.497_2

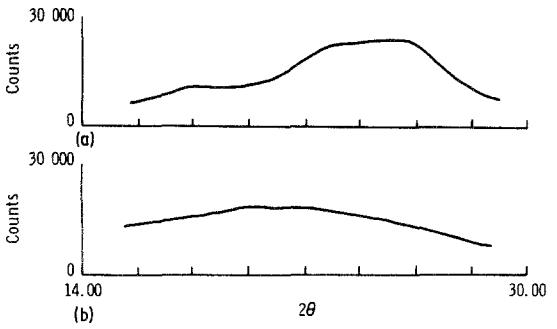

Figure 2 Radial X-ray diffraction patterns determined with PSPC in the horizontal position: (a) Sample A906 (ET = 90° C, λ = 4.2); (b) sample A502 (ET = 50° C, λ = 2.5). Scanned in the equatorial direction (perpendicular to direction of elongation).

where

$$\langle\cos^2\varepsilon\rangle = 0.8807\langle\cos^2\phi_{010}\rangle + 0.7755\langle\cos^2\phi_{T10}\rangle - 0.6562\langle\cos^2\phi_{100}\rangle \quad (11)$$

$$f_{x,c} = \tfrac{1}{2}[3\langle\cos^2\sigma\rangle - 1] \quad (12)$$

where

$$\langle\cos^2\sigma\rangle = 1 - 0.8807\langle\cos^2\phi_{010}\rangle - 0.7755\langle\cos^2\phi_{T10}\rangle - 0.3438\langle\cos^2\phi_{100}\rangle \quad (13)$$

3. Results and discussion

To elucidate the development of oriented states in the coextrusion process, both amorphous and crystallite orientation have been determined as a function of draw ratio, λ, and extrusion temperature, ET. Fig. 2 shows X-ray diffraction scans of PET coextrudates drawn at different λ and ET at higher crystallinity, illustrated in Fig. 1a, the (0 1 0), (T 1 0) and (1 0 0) peaks are evident, but in the case of lower crystallinity these peaks are too weak to be resolved above the amorphous halo (Fig. 2b). As seen in Fig. 3, most of PET coextrudates studied in this work are of relatively low crystallinity. (This crystallinity results from the high elongational stresses in the conical die, as shown by polarized microscopy and small angle X-ray scattering, SAXS.) For this reason an alternate method of evaluating the crystallinity orientation function is required. The crystallite orientation function, f_c, can thus be calculated indirectly by subtracting the dichroism contribution from the overall birefringence.

Figs. 4 to 7 show the relation between f_c and extrusion draw ratio (EDR) λ at several ET. The orientation functions, f_{av} and $f_{a,d}$ are also plotted against λ for comparison. All curves have similar shapes. At levels of extrusion draw ratio up to 2.5, $f_{a,d}$ increases with λ with the rate depending upon ET. The higher value of $\delta f_{a,d}/\delta\lambda$ for an ET below T_g is accounted for by the slower relaxation of amorphous chains and the higher crystallinity in the coextrudate (see also Fig. 3). At $\lambda > 3.0$, $\delta f_{a,d}/\delta\lambda$ increases markedly for all ET, likely associated with the increase of crystallinity (see Fig. 3). The change of $f_{a,d}$ with respect to λ is less as λ approaches ~4.3, corresponding to the natural PET draw ratio in a conventional drawing.

Figs. 4 to 7 show that the change in f_{av} against λ is similar to that of $f_{a,d}$ against λ. At an ET of 90° C they coincide at λ. The average measure of crystalline and amorphous orientation, should approach $f_{a,d}$ when induced crystallization is negligible as in such coextrusions (see Fig. 3).

A major difference appears between the f_c and the $f_{a,d}$ changes with λ. In the ET range of 50 to 70° C, f_c increases almost linearly with λ, even at initial draw. For an ET of 90° C, the crystallinity produced at low draw is too small to evaluate f_c accurately. At a $\lambda > 4$, all f_c against λ curves level off with a f_c value of ~0.9.

Figs. 8 and 9 are plots of f_c and $f_{a,d}$ against f_{av} for samples prepared at temperatures below and above T_g respectively. Within the range studied, the order $f_c > f_{av} > f_{a,d}$ is observed. This agrees with the results obtained by Okajima *et al.* [14], but differ from Matsuo *et al.* [9]. Both investigated the oriented state of conventionally drawn PET. Our results on solid state coextrudates show that PET crystalline orientation is always higher than that of the amorphous component. This might be due to a higher rate constant

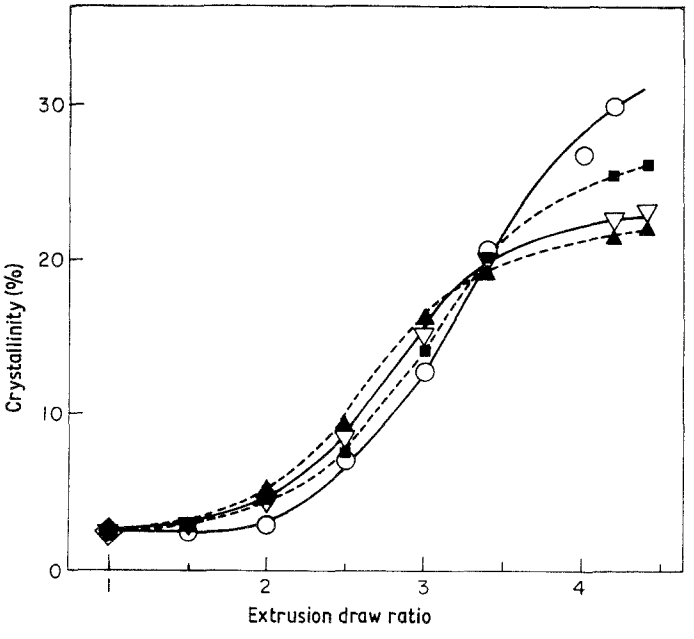

Figure 3 Crystallinity as a function of extrusion draw ratio (▲) ET = 50° C, (▽) ET = 60° C, (■) ET = 70° C, (○) ET = 90° C.

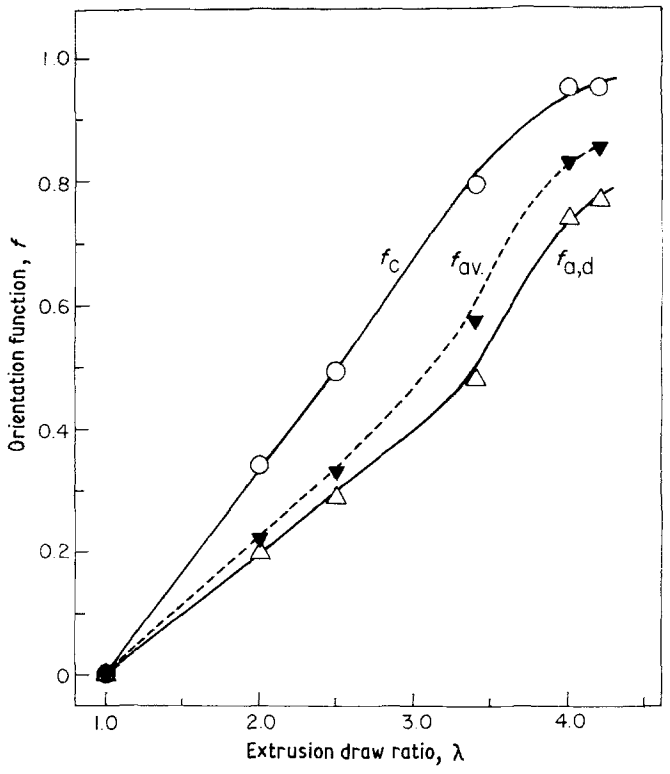

Figure 4 Orientation functions (f_c, $f_{a,v}$ and $f_{a,d}$) as a function of extrusion draw ratio at ET = 50° C.

and lower activation energy for cold crystallization in the extrusion process [11]. No significant difference in f_c against f_{av} and $f_{a,d}$ against f_{av} plots is observed for ET variation (below T_g) (Fig. 8). However, when ET $> T_g$ (Fig. 9), f_c is higher and $f_{a,d}$ is reduced as ET is increased from 70 to 90° C. This may be considered due to more ready relaxation and/or limited orientation of amorphous PET segments at temperatures increasingly above T_g.

Fig. 10 shows the relation between the amorphous orientation function, $f_{a,d}$, and crystallite orientation function, f_c, at several ET. At low orientation range, the rate of change of $f_{a,d}$ with respect to f_c at a given extrusion temperature, $\delta f_{a,d}/\delta f_c$, is less than unity, meanwhile it decreases with increasing extrusion temperature. At high orientation this tendency is reversed, i.e. $\delta f_{a,c}/\delta f_c > 1$. This suggests that initially on drawing the increase of crystallite orientation is mainly the result of crystallization induced by the most highly oriented amorphous fraction. The thermal relaxation of less oriented uncrystallized amorphous fractions must be more prominent at higher ET. At higher λ, the higher elongational stress leads to more crystallinity, with the stress-induced crystallites playing the role of

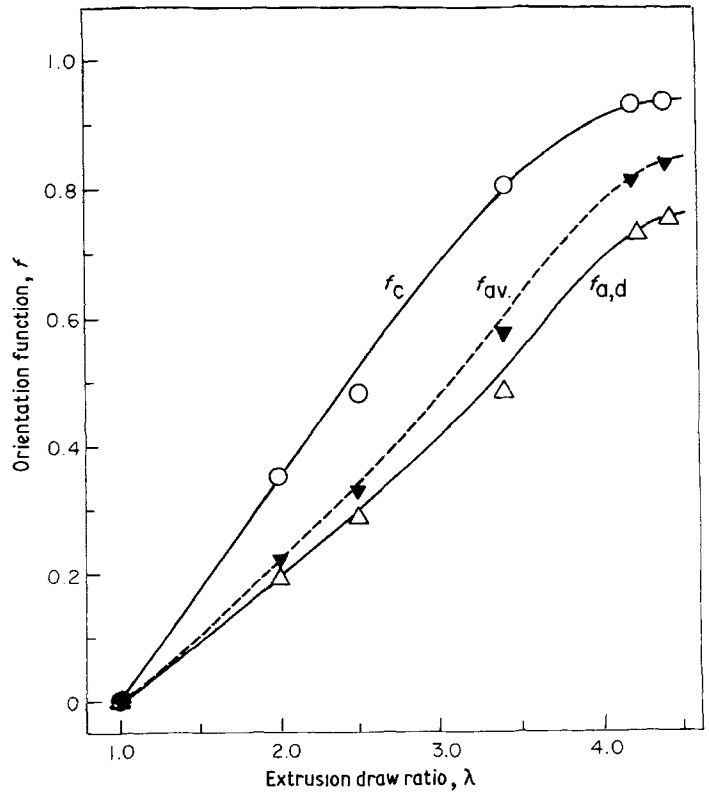

Figure 5 Orientation functions (f_c, $f_{a,v}$ and $f_{a,d}$) as a function of extrusion draw ratio at ET = 60° C.

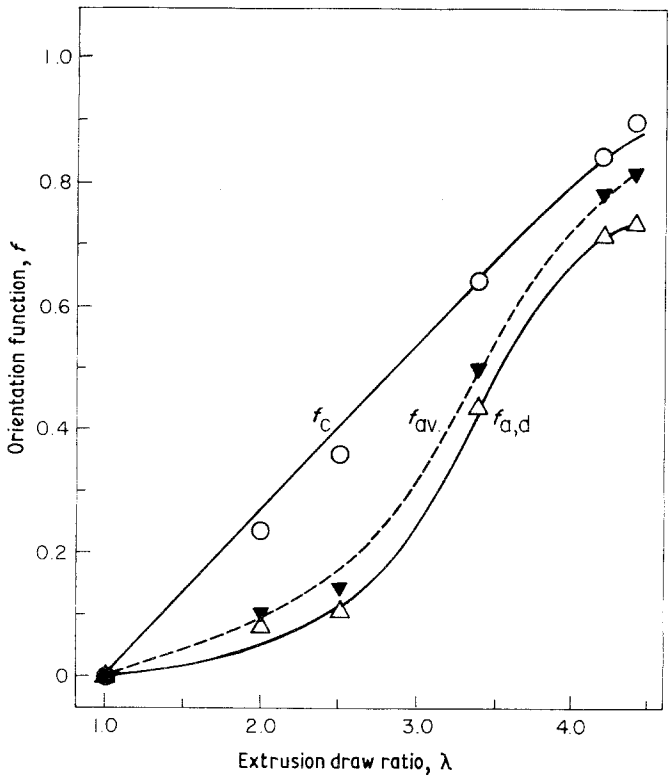

Figure 6 Orientation functions (f_c, $f_{a,v}$ and $f_{a,d}$) as a function of extrusion draw ratio at ET = 70° C.

a physical crosslink. This feature could restrict further orientation of amorphous components. A restriction on the rate of increase of f_c with λ can be due to the saturation of crystalline orientation. It is of note that at high orientation, $\delta f_{a,d}/\delta f_c$ is larger than unity, but even in this case the relation $f_c > f_{a,d}$ still holds (see Fig. 10).

The calculated crystalline orientation function, f_c, has also been compared with the orientation functions of the three principal crystallite axes, $f_{x,a}$, $f_{x,b}$ and $f_{x,c}$ evaluated directly from X-ray diffraction. Fig. 11 shows the X-ray diffraction spectra of highly-drawn PET. A major difference appears in the coextrudates made below and above T_g. The former (Fig. 11b) exhibits very small and/or imperfect crystallites, so that the (0 1 0), (T1 0) and (1 0 0) peaks are not resolved. The coextrudate prepared at 90° C shows the three diffraction lines resolved quite well. For those samples for which the (0 1 0), (T1 0) and (1 0 0) peaks are unresolved, $f_{x,c}$ was obtained by the following way. Sample A706 is taken as an example, see Fig. 11b, a broad peak is seen with its maximum in the approximate (1 0 0) position. The orientation function determined at this position is denoted by $\langle \cos^2 \phi_{100} \rangle$, and thus

$$\langle \cos^2 \phi_{100} \rangle = \frac{2f_{100} + 1}{3} \qquad (14)$$

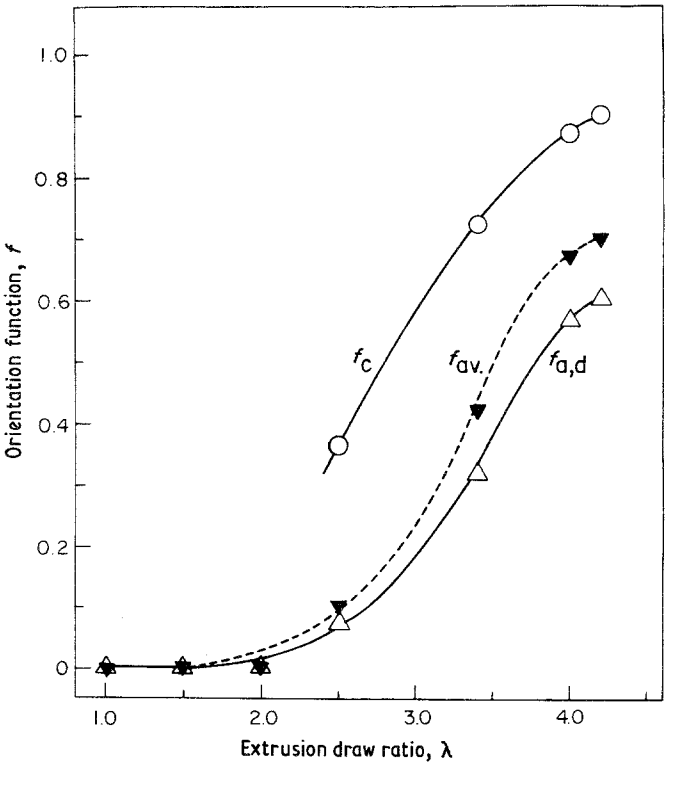

Figure 7 Orientation functions (f_c, $f_{a,v}$ and $f_{a,d}$) as a function of extrusion draw ratio at ET = 90° C.

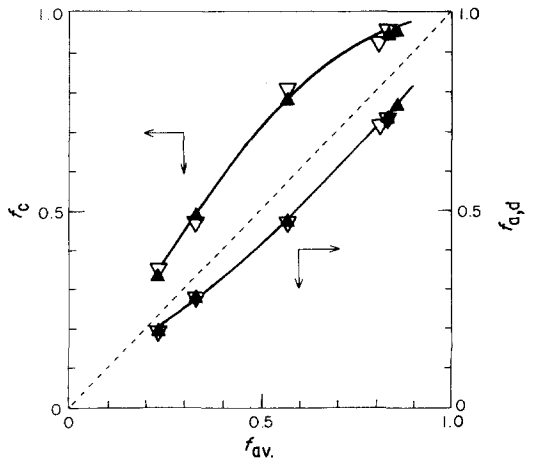

Figure 8 f_c and $f_{a,d}$ as a function of $f_{a,v}$: (▲) ET = 50° C, (▽) ET = 60° C.

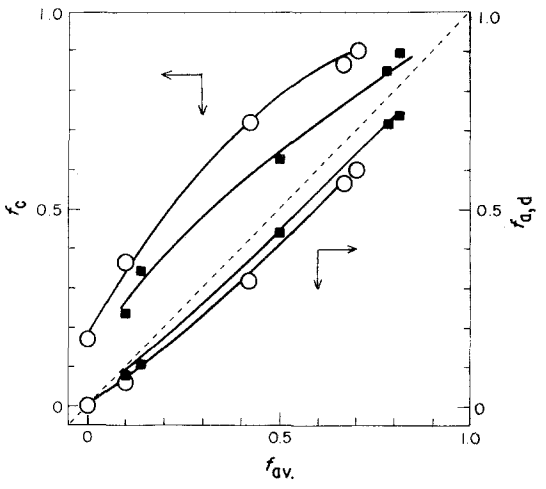

Figure 9 f_c and $f_{a,d}$ as a function of $f_{a,v}$ (■) ET = 70° C, (○) ET = 90° C.

Assuming infinite rotational symmetry about the crystal c-axis, so that

$$\langle \cos^2 \delta \rangle = \langle \cos^2 \varepsilon \rangle = \langle \cos^2 \phi_{100} \rangle \quad (15)$$

$\langle \cos^2 \delta \rangle$ and hence $f_{x,c}$ can be obtained readily by orthogonality. Again, as in the case of Fig. 11b, for sample A606 (EDR = 4.4, ET = 60° C), $f_{x,c}$ has been evaluated in the same way.

The orientation functions of the three principal crystallites axes are listed with f_c and $f_{a,d}$ in Table II. At high λ, orientation functions of the principal axes show an almost perfect orientation along the stretch direction. Within the range studied $f_{x,c}$ is always greater than f_c, again suggesting that the higher the lateral order, the more prominent the orientation. For an ET below T_g (see sample A606 in Table II), $f_{x,c}$ and f_c are similar. This implies that in solid state coextrusion, the stress-induced crystallites formed below T_g are more imperfect. As reported by Mayban *et al.* [19] and Ito *et al.* [20], below T_g, but above 50° C, PET exhibits certain minor segment motions. In our previous work [11] it was also found that such motion could lead to packing of the oriented amorphous segments into a crystalline lattice, even below T_g, thus depressing the cold crystallization temperature. It is plausible that such crystallites could be less perfect due to insufficient thermal segment motion in stress-induced crystallization. The ET dependence of $f_{a,d}$, but the independence of $f_{x,c}$ and f_c, show the greater tendency of thermal relaxation of amorphous chains, particularly at an ET $> T_g$. The similar and high values of $f_{x,c}$ and $f_{a,d}$ suggest a higher deformation efficiency during solid state coextrusion as compared with conventional drawing [14]. The reasonable agreement of $f_{x,c}$ with f_c also suggests that the orientation evaluations used here are internally consistent.

4. Conclusions

1. By using solid state coextrusion uniformly drawn films have been prepared at a series of draw ratios from glassy amorphous PET.

2. The dichroism and birefringence on the drawn PET have been determined to obtain $f_{a,d}$ directly and f_c deductively. For more crystalline samples, $f_{x,a}$, $f_{x,b}$ and $f_{x,c}$ were also obtained from X-ray diffraction and found to compare favourably with values from dichroism and birefringence.

3. Both amorphous and crystalline orientations are developed more efficiently by solid state coextrusion than by conventional drawing.

4. The dye molecules incorporated in PET likely resides only in the fraction of amorphous matrix of lower lateral order. Therefore, $f_{x,c}$, f_c and $f_{a,d}$ should reflect the corresponding orientation functions of various order (i.e. crystalline, crystalline combined with high lateral order and lower lateral order respectively). The relation $f_{x,c} > f_c > f_{av} > f_{a,d}$ holds well, indicating that the higher the lateral order, the more prominent the orientation.

5. The trend $f_{x,c} > f_c > f_{a,d}$ may not only be due to the greater orientation tendency of crystalline regions, but also to the greater tendency for cold crystallization on coextrusion drawing of amorphous PET.

6. In the range of low orientation, the rate of crystalline orientation with respect to draw ratio is greater than that of the amorphous component. ($\delta f_{a,d}/\delta f_{a,d} < 1$). For higher orientations, this tendency is reversed (i.e. $\delta f_{a,d}/\delta f_c > 1$). This is due to the saturation of crystalline orientations at high draw ratio as well as the constraint of oriented amorphous segments by the crystallites embedded with the amorphous matrix.

7. The observed relation, $f_{x,c} \geqslant f_c$ as ET $\gtrless T_g$

TABLE II Orientation functions of the three principal crystallographic axes and amorphous matrix

Sample no.	Extrusion draw ratio	Extrusion temperature (° C)	$f_{x,a}$	$f_{x,b}$	$f_{x,c}$	f_c	$f_{a,d}$
A606	4.4	60	−0.47	−0.47	0.94	0.93	0.75
A706	4.4	70	−0.48	−0.48	0.96	0.90	0.73
A906	4.2	90	−0.49	−0.47	0.96	0.90	0.60

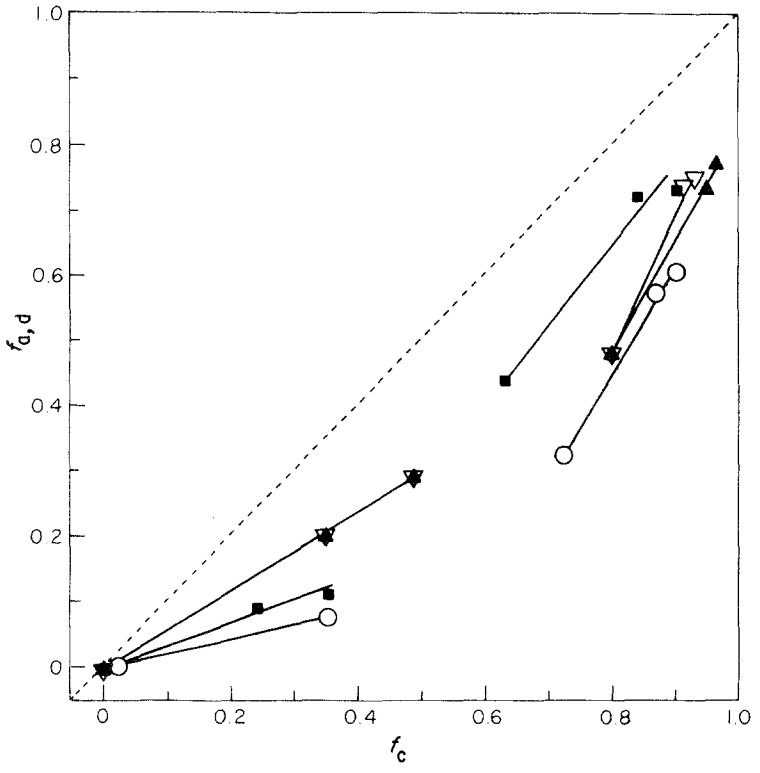

Figure 10 $f_{a,d}$ as a function at various extrusion temperatures (▲) 50° C, (▽) 60° C, (■) 70° C, (○) 90° C.

respectively, implies that in solid state coextrudates, prior to annealing, the crystallites formed below T_g are imperfect, likely due to insufficient thermal motion in stress-induced crystallization. This is consistent with the difficult resolution of the (0 1 0), (T 1 0) and (1 0 0) lines in X-ray diffraction spectra.

8. When an amorphous and isotropic PET is used for solid state extrusion, the elongational stress created in a conical die extends, orders and orients the macromolecular segments gradually and continuously with increasing extrusion draw ratio in tests both below and above T_g. The orientation of the amorphous segments reaches a plateau, and a fraction of it is converted into crystals. The crystallites so generated are highly oriented and less perfect for drawing below T_g.

References

1. J. R. C. PEREIRA and R. S. PORTER, *J. Polym. Sci., Polym. Phys. Ed.* **21** (1983) 1133.
2. T. SUN, T. KYU, J. SHENG, D. LEFEBVRE, R. S. STEIN and R. S. PORTER, *J. Appl. Polym. Sci.* **30** (1985) 251.
3. J. E. SPRUIELL, D. E. McCORD and R. A. BEUERLEIN, *Trans. Soc. Rheol.* **16** (1972) 535.
4. W. J. DULMUGE and A. L. GEDDES, *J. Polym. Sci.* **15** (1958) 499.
5. G. FARROW and J. BAGLEY, *J. Text. Res.* **32** (1962) 587.
6. C. J. HEFFELFINGER and P. G. SCHMIDT, *J. Appl. Polym. Sci.* **9** (1965) 2261.
7. J. H. DUMBLETON and B. B. BOWLES, *J. Polym. Sci. Pt. A-2* **4** (1966) 951.
8. A. MISRA and R. S. STEIN, *J. Polym. Sci., Polym. Phys. Ed.* **17** (1979) 235.
9. M. MATSUO, M. TAMADA, T. TERADA, C. SAWATARI and M. NIWA, *Macromolecules* **15** (1982) 988.
10. T. TERADA, C. SAWATARI, T. CHIGONO and M. MATSUO, *ibid.* **15** (1982) 998.
11. T. SUN, J. R. C. PERIRA and R. S. PORTER, *J. Polym. Sci., Polym. Phys. Ed.* **22** (1984) 1163.
12. J. H. DUMBLETON, *J. Polym. Sci., Pt. A-2* **6**, (1968) 795.
13. K. NAKAYAMA, S. OKAJIMA and Y. KABAYASHI, *J. Appl. Polym. Sci.* **13** (1969) 659.
14. S. OKAJIMA, K. NAKAYAMA, K. KAYAMA and Y. KATO, *ibid.* **14**, (1970) 1069.
15. C. R. DESPER, J. H. SOUTHERN, R. D. ULRICH and R. S. PORTER, *J. Appl. Phys.* **41** (1970) 4284.
16. W. R. BUSING and H. A. LEVY, *Acta Crystallogr.* **22** (1967) 457.
17. S. KOJIMA, C. R. DESPER and R. S. PORTER, *J. Polym. Sci., Polym. Phys. Ed.* **16** (1978) 1721.
18. Z. WILCHINSKY, *Adv. X-ray Anal.* **6** (1963) 231.
19. K. G. MAYBAN, W. J. JAMES and W. BASCH. *J. Appl. Polym. Sci.* **9** (1965) 3605.
20. E. ITO, K. YAMAMOTO, Y. KOBAYASHI and T. HAFAKEYAMA, *Polymer* **19** (1978) 39.

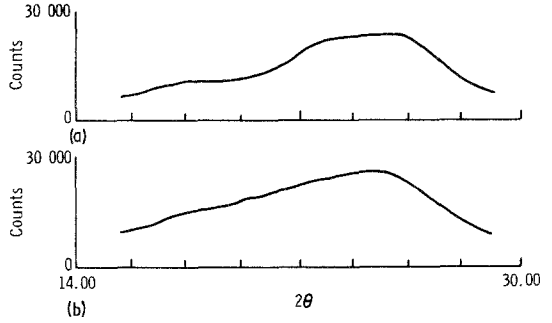

Figure 11 Equatorial radial X-ray diffraction patterns: (a) sample A906 (ET = 90° C, λ = 4.2); (b) sample A706 (ET = 70° C, λ = 4.4).

Received 1 September
and accepted 1 October 1985